Computer simulation of structures and cohesive properties of micas

David R. Collins

Department of Chemistry, University of Keele, Keele, Staffordshire ST5 5BG, U.K.

C. Richard A. Catlow

Davy Faraday Research Laboratory, The Royal Institution, 21 Albemarle Street, London W1X 4BS, U.K.

Abstract

Computational energy minimization and free-energy minimization techniques have been used to study the structures and crystal properties of muscovite, phlogopite, and several octahedrally substituted phlogopite analogues. These simulations employ ionic potential models that include three-body O-Si-O bond-bending terms. The calculated structures of these micas are in acceptable agreement with experiment. Moreover, the elastic and dielectric constants and the acoustic phonon properties of muscovite are in close agreement with experiment, thereby demonstrating the applicability of the techniques and potential models to this class of material. The effects of divalent octahedral cation substitution on the structure of phlogopite are also studied.

Introduction

In this paper, we report a detailed study of the structures and properties of micas using computer modeling methods. Our studies are motivated by an incomplete understanding of the structural, physical, and chemical properties of micas. Many micas have proved difficult to study experimentally, often because of the lack of pure well-ordered single crystals. However, owing to increased sophistication of simulation techniques and growing computer power, there has been considerable expansion in modeling studies of silicates in recent years (Catlow and Cormack, 1987), and it is now clear that a large number of silicate structures and properties can be modeled accurately.

Previous theoretical studies of micas and other layered silicates have often considered only electrostatic interactions, neglecting contributions from short-range forces. Such studies have included the modeling of OH orientations in a number of 2:1 phyllosilicates (Giese, 1979) and an estimation of the magnitude of interlayer bonding in muscovite (Giese, 1974). Electrostatic calculations have also been used to study the energetics of intercalation processes in vermiculite (Jenkins, 1982). This work also investigated energies of transition between dioctahedral and trioctahedral layered silicates, as well as hydroxyl to fluoro transitions, using lattice energy calculations, but without minimization procedures. Recently, calculations based purely on electrostatic interactions have been used to investigate polytypism in micas by attempting to discriminate energetically among alternative model structures (Abbott and Burnham, 1988).

Early applications of energy minimization to inorganic systems concerned simple oxides (see, e.g., Catlow, 1977). The technique has been applied successfully to a much wider range of materials, including silicates, over the last 5 yr. Earlier uses of energy minimization simulations gen-erally concerned anhydrous close-packed high-temperature and high-pressure minerals such as olivine (Parker and Price, 1985), garnets (Parker, 1982), and pyroxenes (Catlow et al., 1982b). More recently the techniques have been applied to the simulation of open-framework zeolites (Sanders, 1984; Sanders et al., 1984; Hope, 1985; Jackson and Catlow, 1988), and feldspar structures (Purton and Catlow, 1990).

Free-energy minimization simulations are a recent development. They require calculations of the properties of lattice dynamics as well as lattice statics. To date, work using these methods has focused on the stability of SiO_2 polymorphs and forsterite (Parker and Price, 1989), the prediction of the phase diagram of the latter being a notable achievement.

In this paper we report the results of simulations of several micas whose structures and chemical composition are well known, which enabled us to make detailed comparisons with experimental data and thereby to assess the extent to which the techniques and the potential models are suitable for micas and silicates. We concentrate on the micas muscovite and phlogopite and some octahedrally substituted analogues of the latter. We compare experimental and calculated structures, referring to unit-cell dimensions, bond lengths, and polyhedral distortions, plus the experimental and calculated phonon dispersion curves and elastic constants of muscovite. Our calculations reveal a generally good agreement between simulated and experimental results, although detailed discrepancies point to the need for some refinement of the interatomic potentials used.

Simulation techniques

The computer simulation techniques used is this work employ a classical description of the crystal structure based on the Born model (Born and Huang, 1954). The poten-

tial model describing the effective forces acting between the atoms in the structure has the following four components:

1. There is an electrostatic term, which is evaluated using the Ewald transformation (Ewald, 1921; Tosi, 1964).

2. A two-body short-range term describes repulsions from electron cloud overlap and attractions due to dispersion and covalence. In this study we describe cation-O and the O-O interactions using a Buckingham function: $U_{sr} = A \exp(-r/\rho) - Cr^{-6}$, where the exponential term describes the repulsive energy and the r^{-6} term the longer range attraction. The intramolecular OH interaction is represented by a Morse function: $U_{sr} = D_e\{1 - \exp[-\beta(r - r_e)]\}^2$, where r and r_e are the observed and equilibrium interatomic distances, respectively. Coulomb forces are not included between atoms coupled by a Morse potential, as it is assumed that this potential describes all components of the interactions between the two atoms. As in many previous simulation studies on silicates, the short-range cation-cation interactions are not significant and were therefore neglected.

3. A three-body short-range term describes angular dependent covalent forces. A simple approach (see, e.g., Catlow and Cormack, 1987) is to include bond-bending terms about the tetrahedral cation of the type $U_{thb} = \frac{1}{2}K_{thb}(\theta - \theta_O)^2$, where K_{thb} is the harmonic three-body force constant, and θ and θ_O are the observed and ideal tetrahedral O-T-O bond angles, respectively.

4. A term to describe electronic polarizability is required if dielectric and dynamic properties are to be modeled accurately. In this study we used the shell model (Dick and Overhauser, 1958), which provides a simple mechanical model of electronic polarizability. The core-shell self energy is given by $U_s = \frac{1}{2}K_s r^2$, where K_s is the harmonic spring constant and r is the core-shell separation. The development of a dipole moment is described in terms of the displacement of the shell relative to the core. The free-ion electronic polarizability, α, is given by $\alpha = Y^2/K_s$, where Y is the shell charge.

In order to predict the minimum energy configuration of a crystal structure, the lattice energy calculations must be coupled to a minimization procedure. We have used the computer code THBREL (Leslie, in preparation) which employs a Newton-Raphson algorithm. Such calculations can be performed either with fixed (constant-volume) or, as in this study, variable (constant-pressure) unit-cell dimensions. Detailed discussions of the methods are available elsewhere (see, e.g., Norgett and Fletcher, 1970; Catlow and Mackrodt, 1982).

The elastic constant tensor C_i is calculated analytically using standard procedures, which require the prior calculation of the second derivatives of the total lattice energy with respect to the six bulk strain components and with respect to atomic coordinates. The formalisms employed are described in detail elsewhere (Catlow and Norgett, 1976; and Catlow and Mackrodt, 1982; Parker and Price, 1989, 1990) and summarized in Appendix 1.

Following energy minimization, the vibrational properties of the structure can be calculated using a lattice dynamical approach. Such procedures have been described in detail previously (Born and Huang, 1954; Ziman, 1964; Cochran, 1973) and discussed in the context of atomistic simulations in a number of recent studies (Parker and Price, 1989, 1990). The vibrational frequencies of a lattice are related to the static energy by $m\omega^2(\mathbf{q}) = \mathbf{D}(\mathbf{q})\mathbf{e}(\mathbf{q})$, where m is the atomic mass, $\mathbf{q}$ is the reciprocal lattice wavevector of the lattice vibration, $\omega(\mathbf{q})$ is the frequency of the vibrational modes, and $\mathbf{D}(\mathbf{q})$ is the dynamical matrix, given by $\mathbf{D}(\mathbf{q}) = \Sigma_{i,j} (\partial^2 U/\partial \mathbf{u}_i \partial \mathbf{u}_j) \exp(i\mathbf{q}\cdot\mathbf{R})$, where $\mathbf{R}$ is the interatomic separation, and $\mathbf{u}_i$ and $\mathbf{u}_j$ are the atomic displacements from equilibrium positions. For a unit cell containing N atoms, there are $3N$ solutions for a given value of $\mathbf{q}$. We have used the computer code THBPHON (Leslie, in preparation) to calculate within the harmonic approximation the eigenvalues $[\omega^2(\mathbf{q})]$ from which the vibrational frequencies are derived. In addition the program also calculates the eigenvectors $[\mathbf{e}_x(\mathbf{q}), \mathbf{e}_y(\mathbf{q}), \mathbf{e}_z(\mathbf{q})]$, which describe the pattern of atomic displacements for each vibrational mode.

From a knowledge of the phonon frequencies over the entire Brillouin zone, the phonon density of states may be determined, which in turn can be used to calculate a number of thermodynamic properties. For example, the vibrational free energy (F_{vib}) is given by $F_{vib} = kT\Sigma_i^M[\chi/2 + \ln(1 - e^\chi)]$, where $\chi = \hbar w_i/kT$, in which ω_i is the frequency of the ith mode, k is Boltzmann's constant, and T is the absolute temperature. The summation is carried out over the total number of phonon frequencies, M.

Recently free-energy minimization simulations have been embodied in the computer code Parapocs (Parker and Price, 1989, 1990), which simulates crystal structures and hence dynamical properties at temperatures above 0 K. The effects of thermal expansion are included using the quasi-harmonic approximation, which accounts for thermal expansion by calculating the volume dependence of vibrational frequencies and hence of thermodynamic properties. The technique involves minimizing the Helmholtz free energy ($U + F_{vib}$), rather than simply the internal energy (U), as in energy minimization. During the minimization both cell dimensions and atomic coordinates are varied. Within the quasi-harmonic approximation a nested minimization procedure is employed, i.e., for each set of cell dimensions, the atomic coordinates are adjusted to zero strain; the cell dimensions themselves are varied until the value of $dF/d\epsilon_j$ is zero for all six bulk strains ϵ_j. The latter derivatives are calculated numerically by applying small additional strains in each of the six directions. Full details are given elsewhere (Parker and Price, 1989, 1990).

PARAMETERIZATION OF INTERATOMIC POTENTIALS

Accurate interatomic potentials are an essential prerequisite for reliable atomistic simulations. Parameterization may be achieved by both empirical fitting and theoretical procedures. The latter range from the electron gas methods (Gordon and Kim, 1972), which have been widely

TABLE 1. Short range potential parameters

	Two-body short-range interaction			Reference
	A/eV	ρ/Å	C/eV Å^{-6}	
Si^{4+}-O^{2-}	1283.9	0.3205	10.6	a
Si^{4+}-$O^{1.426-}$(H)	999.9	0.3012	0.0	b
Al^{3+}-O^{2-}	1460.3	0.2991	0.0	c
K^{+}-O^{2-}	65269.7	0.2130	0.0	d
Mg^{2+}-O^{2-}	1275.2	0.3012	0.0	e
Ni^{2+}-O^{2-}	683.5	0.3332	0.0	f
Mg^{2+}-O^{2-}	821.6	0.3242	0.0	f
Co^{2+}-O^{2-}	696.3	0.3362	0.0	f
Fe^{2+}-O^{2-}	694.1	0.3399	0.0	f
Zn^{2+}-O^{2-}	499.6	0.3595	0.0	f
Mn^{2+}-O^{2-}	715.8	0.3464	0.0	f
Cd^{2+}-O^{2-}	868.3	0.3500	0.0	f
O^{2-}-O^{2-}	22764.0	0.149	27.88	a
	D_e/eV	β/Å^{-1}	r_e/Å	Reference
$H^{0.426+}$-$O^{1.426-}$	7.0525	2.1986	0.9485	g

Shell model interaction

	Y|e|	K/eV Å^{-2}	Reference
O^{2-}	−2.8690	74.92	a

Three-body interaction

	K_b/eV rad^{-2}	θ_0/°	Reference
O^{2-}-Si^{4+}-O^{2-}	2.09724	109.47	a

Note: a = Sanders et al. (1984), b = Catlow et al. (1982b), c = Catlow et al. (1982a), d = Post and Burnham (1986), e = Sangster and Stoneham (1981), f = Lewis and Catlow (1985), g = Saul et al. (1985); a–d are fitted to a Buckingham function, $U = A \exp(-r/\rho) - Cr^{-6}$; e is fitted to a Coulombic-subtracted Morse function, $U = D_e\{1 - \exp[-\beta(r - r_e)]\} - qqr^{-1}$. Y = shell charge; K = interatomic force constant; K_B = bond-bending force constant; θ_0 = equilibrium bond angle.

used by a number of workers (see, for example, Mackrodt and Stewart, 1979; Post and Burnham, 1986), to ab initio Hartree-Fock techniques, which have recently been applied to the study of silicate potentials (Lasaga and Gibbs, 1987; van Beest et al., 1990). Although a physical significance can be attached to theoretically derived potential parameters, it is reduced when empirical fitting procedures are used. Indeed if sufficient parameters are fitted, then physical significance may be largely lost. In this study we have used interatomic potentials that have been transferred from a number of previous studies (see Table 1). All the potentials employ full integral charges on all atoms, except for the OH species ($q_O = -1.426$, $q_H = +0.426$) whose sum equals −1 but whose component atoms have partial charges chosen so as to reproduce the dipole moment of the OH group (Saul et al., 1985).

The short-range potentials for all tetrahedral atoms (i.e., both Si and Al) in our model are taken to be those of the Si atom. They include the three-body O-Si-O bond-bending potential (Sanders et al., 1984), which has been used to model accurately structures and crystal properties of almost every major group of rock-forming silicate minerals (see, e.g., Price et al., 1987; Wall and Price, 1988; Dove, 1989; Purton and Catlow, 1990).

The other short-range interactions include an empirical two-body Si-O potential (Catlow et al., 1982b), for O

atoms that are part of the OH group; an empirical Al-O potential (Catlow et al., 1982a), where Al is in the octahedral sites; and an electron gas K-O potential (Post and Burnham, 1986). The Mg-O potential used in most simulations of phlogopite was fitted empirically to the structure and dielectric properties of MgO (Sangster and Stoneham, 1981). In our study of octahedrally substituted phlogopite analogues, we used potentials that were derived as a consistent set (Lewis, 1984; Lewis and Catlow, 1985). These were derived, using empirical fitting procedures, to a range of oxides including NiO, MgO, CoO, FeO, and MnO. We note that the potential parameters for MgO in this set differ from those employed by Sangster and Stoneham (1981). A Cd-O interaction that had been calculated from an extrapolation procedure (Lewis and Catlow, 1985) was also used in this study. We used an O-O potential calculated ab initio (Catlow, 1977), but with a dispersion term and shell parameters that were fitted empirically (Sanders et al., 1984). The O-H potential used to describe the intramolecular interaction of the hydroxide was calculated ab initio (Saul et al., 1985). The longer range H bonds (OH-O) interact purely by electrostatic forces.

The distribution of Al,Si in the tetrahedral sites in $2M_1$ muscovite and $1M$ phlogopite generally shows no long-range ordering (Bailey, 1975, 1984). The explicit inclusion of $^{[4]}$Al and $^{[4]}$Si in simulations would therefore violate the accepted space group symmetry by incorrectly imposing long-range ordering. Following a previous simulation study of muscovite (Collins and Catlow, 1990), we continue to use a single hybrid species ($Al_{0.25}Si_{0.75}$) of both charge (+3.75) and mass (27.81) to represent the tetrahedral cations, with the short-range interactions of Si. Although the atomic vibrations of this species are not identical to the average of Al and Si in the whole crystal, the difference is probably small, since Al and Si are adjacent in the periodic table. The errors introduced by this approximation would not be expected to be large for disordered materials.

RESULTS

Muscovite

Structure. Simulated structural parameters of muscovite are compared with experimental data (Rothbauer, 1971; Knurr and Bailey, 1986) in Table 2. Unit-cell dimensions, bond lengths, and distortions of simulated structures at 0 and 300 K were all found to be in good agreement with experimental values. Two experimental structures are given to show that, although structural parameters of individual muscovite crystals can be measured very accurately, the variation of parameters between crystals is significant, that being a consequence of differences in chemical composition. These differences should be borne in mind when comparing simulated values with experiments.

The important features of Table 2 are summarized as follows:

1. The energy-minimized and free-energy-minimized

unit-cell dimensions are all within 2% (and in most cases 1%) of experiment.

2. The c-axis lattice parameter of the free-energy-minimized structure at 300 K shows an improved agreement with experiment when compared to the energy-minimized (0 K) structure; the experimental data refer to room temperature. We note the contrasting response of the cell dimensions to an increase in temperature; the a and b lattice parameters increase by far less between 0 and 300 K than the c lattice parameter. This is a consequence of the bonding between the layers being much weaker than that within the layers. Indeed it is the increase in interlayer separation that is mainly responsible for the large expansion along $\mathbf{c}$, as the thickness of both the tetrahedral and octahedral sheets varies little between 0 and 300 K. The response of the different cation-O bond lengths to temperature is, as expected, similar to that of the sheet thickness and interlayer separation. The K-O bond length increases significantly between 0 and 300 K, whereas both the tetrahedral $Si_{0.75},Al_{0.25}$-O and octahedral Al-O bond lengths vary little over this temperature range. Free-energy simulations over a temperature range of 100–800 K predict considerable anisotropy in the thermal expansion of muscovite. However, we overestimate this effect: we predict the expansion in the c lattice parameter to be almost an order of magnitude greater than that in the a and b lattice parameters, whereas experimental data over a similar temperature range for muscovite (Guggenheim et al., 1987) and phlogopite (Takeda and Morosin, 1975) reveal an anisotropy in the thermal expansion of 1.5 and 2, respectively.

3. The mean T-O bond length is modeled well (within 0.02 Å), indicating the validity of using the Si-O short-range potential to represent the interaction of the hybrid species with O.

4. The O_{basal}-T-O_{apical} bond angles, τ, are calculated to be slightly less than the ideal undisturbed value of 109.47° whereas the experimental value is a little greater. The K-O potential is probably slightly too repulsive, causing the basal O atoms to be pushed back into the tetrahedral sheet.

5. The tetrahedral rotation angle, α, is underestimated and therefore the difference, Δ, between K-O_{outer} and K-O_{inner}, is also underestimated.

6. The measure of departure from coplanarity of the basal O atoms, ΔZ, (corrugation of the basal surfaces) is correctly predicted to be appreciable.

7. The mean Al-O,OH bond length is modeled very well, as is the octahedral flattening angle, ψ.

8. The calculated OH bond length is close to experiment.

9. The modeling of the interlayer region, that is, the K-O_{inner} and K-O_{outer} bond lengths, and the difference between them, Δ, is dependent on not only the K-O interactions but also the amount of tetrahedral rotation, α, due to the sheet misfit. As α increases, so does Δ (i.e., K-O_{inner} becomes smaller, and K-O_{outer} becomes larger). Since the tetrahedral rotation arises from the misfit be-

TABLE 2. Comparison of simulated and experimental structural parameters of $2M_l$ muscovite

	Expt.*	Expt.**	0-K sim.	300-K sim.
Cell dimensions				
a	5.192	5.204	5.246	5.254
b	9.0153	9.018	9.179	9.195
c	20.046	20.073	19.783	20.009
β	95.73	95.82	96.53	96.53
Thickness				
Tet sheet	2.245	2.243	2.234	2.238
Oct sheet	2.089	2.106	2.109	2.113
Interlayer separation	3.393	3.393	3.250	3.359
Tet sheet				
Mean T-O	1.644	1.644	1.620	1.622
τ	110.9	111.0	107.5	107.6
α	11.3	10.8	7.6	7.5
ΔZ	0.21	0.22	0.33	0.32
Oct sheet				
Mean M2-O,OH	1.930	1.934	1.932	1.934
ψ(M2)	57.2	57.0	56.9	56.9
O-H	—	0.920	0.975	0.975
Interlayer separation				
K-O_{outer}		3.353	3.331	3.354
K-O_{inner}		2.872	2.980	3.020
Δ		0.481	0.351	0.334

Atomic coordinates (0-K sim.) in $C2/c$			
	x	y	z
T1	0.4662	0.9294	0.1374
T2	0.4506	0.2567	0.1376
M2	0.2711	0.0848	0.0000
K	0.0000	0.0988	0.2500
O1 core	0.4766	0.9557	0.0538
shell	0.4776	0.9566	0.0566
O2 core	0.3523	0.2479	0.0539
shell	0.3523	0.2484	0.0567
O3 core	0.4330	0.0919	0.1723
shell	0.4370	0.0918	0.1663
O4 core	0.2493	0.8112	0.1565
shell	0.2421	0.8166	0.1532
O5 core	0.2456	0.3624	0.1732
shell	0.2400	0.3591	0.1672
OH	0.4717	0.5440	0.0532
H	0.4032	0.6220	0.0794

Note: All lengths in ångströms and angles in degrees. Simulations: $KAl_2AlSi_3O_{10}(OH)_2$.
* Rothbauer (1971): $K_{0.85}Na_{0.1}(Al_{1.81},Fe^{2+}_{0.14},Mg_{0.12})(Al_{0.9}Si_{3.1})O_{9.8}(OH)_2$.
** Knurr and Bailey (1986): $K_{0.93}Na_{0.05}(Al_{1.72},Mn^{3+}_{0.02},Fe^{3+}_{0.149})Al_{0.945},Si_{3.055}O_{10}(OH)_2$.

tween tetrahedral and octahedral sheets, its simulation depends on the interactions of species within these sheets. Therefore, interactions within the tetrahedral and octahedral sheets have a significant influence on the simulated interlayer configuration. Indeed it has been proposed (McCauley and Newnham, 1971) that the interlayer configuration, Δ, is controlled mainly by the sheet misfit and not by the interlayer cation itself. The underestimation of Δ, and the discrepancies in the K-O bond lengths cannot therefore be solely attributed to the K-O short-range potential but are also due to the underestimation of α.

Overall, the reproduction of the properties of muscovite is most satisfactory although the small discrepancies summarized above indicate the need for refinements in the interatomic potential models.

Elastic properties. A very limited amount of data on the elastic properties of micas is available, with individual moduli only reported for muscovite. Treating mus-

TABLE 3. Experimental and calculated elastic moduli for muscovite

Elastic stiffness constants 10^{10} Nm^{-2}	Alexandrov and Ryzhova (1961)	Vaughan and Guggenheim (1986)	0-K sim.	300-K sim.
C_{11}	17.80	18.43	22.87	22.85
C_{22}	17.80	17.84	23.27	23.32
C_{33}	5.49	5.91	6.56	5.72
C_{44}	1.12	1.60	1.63	1.03
C_{55}	1.12	1.76	1.73	1.28
C_{66}	6.78	7.24	7.62	7.65
C_{23}	1.45	2.17	2.24	1.62
C_{13}	1.45	2.38	2.50	1.98
C_{12}	1.52	4.83	9.84	9.51
C_{15}		−0.20	−0.19	−0.17
C_{25}		0.39	0.69	0.44
C_{35}		0.12	0.17	0.07
C_{46}		0.05	0.48	0.28

Fig. 1. Calculated and experimentally measured longitudinal acoustic mode along [00ξ] of muscovite. Calculated curves at 0 K (dashed line) and 300 K (solid line). Experimental measurements from Collins et al., 1992 (open circles) and Cebula et al., 1982 (closed circles).

covite in hexagonal symmetry, an incomplete set of elastic moduli were measured using ultrasonic techniques (Alexandrov and Ryzhova, 1961). More recently, the complete set of 13 individual adiabatic stiffness moduli of a natural sample of $2M_1$ muscovite has been measured using Brillouin scattering techniques (Vaughan and Guggenheim, 1986). These experimental values, together with calculated values at 0 and 300 K, are given in Table 3. The orthonormal axes used to describe the elasticity system are defined according to Vaughan and Guggenheim's alternative system, in which **x** is parallel to **a** and **z** is parallel to **c***. This allows comparisons to be made among different polytypes.

A detailed qualitative explanation relating individual moduli to the structure of muscovite is given by Vaughan and Guggenheim (1986). Their approach is used in the discussion which follows, in which we compare calculated and experimental values. (1) The simulated values agree extremely well with experiment, with C_{15} correctly predicted to be negative, indicating that the methodology and the potential model (including hybrid species to represent tetrahedral cations) are generally adequate. Only the off-diagonal element C_{12} differs significantly from its experimental value. (2) The relationship between structure and elasticity is demonstrated clearly by considering only the compressional moduli (C_{11}, C_{22}, and C_{33}). The large acoustic anisotropy, due to the weak interlayer bonding, is reflected by the observation that $C_{11} \sim C_{22} \gg C_{33}$. (3) The simulations show that the intralayer compressional moduli vary only slightly with temperature,

whereas that perpendicular to the layers decreases significantly with increasing temperature, a consequence of the weak interlayer bonding. (4) We correctly model the small departures from hexagonal symmetry: C_{15} and C_{46} are not zero, and the following pairs of moduli are unequal: C_{11} and C_{22}, C_{44} and C_{55}, C_{23} and C_{13}, as they would be in hexagonally symmetric structures.

Table 4 reports the calculated and experimental isotropic averages of the bulk moduli. Again we observe satisfactory agreement between experiment and simulation.

Phonon spectra. To investigate further the interlayer forces present in muscovite, the phonon spectra perpendicular to the layers have been calculated, thereby providing a stringent test of our potential model. Little data are available for muscovite: the longitudinal acoustic mode along the [00ξ] direction is the only branch to be measured experimentally by using inelastic neutron scattering techniques (Cebula et al., 1982; Collins et al., in preparation).

In our calculations, as we have noted, our potential model includes a hybrid tetrahedral species of both charge and mass. The atomic vibrations of this species are not identical to the average of Al and Si in the whole crystal, but the difference is probably small, as discussed earlier. The calculated longitudinal acoustic branches along the [00ξ] wavevector and the experimental longitudinal acoustic modes are shown in Figure 1. We note the excellent agreement between the calculated and experimental results. This further supports the validity of our potential model and provides confidence for future predictive studies on muscovite. The calculated longitudinal and transverse modes propagating along [00ξ] are shown in Figure 2. The shape of these dispersion curves is approx-

TABLE 4. Experimental and calculated isotropic elastic moduli

	Expt. (Vaughan and Guggenheim, 1986)	0-K sim.	300-K sim.
Bulk Modulus (Voigt) 10^{10} Nm^{-2}	6.77	9.20	8.68
Shear Modulus (Voigt) 10^{10} Nm^{-2}	4.31	4.83	4.58
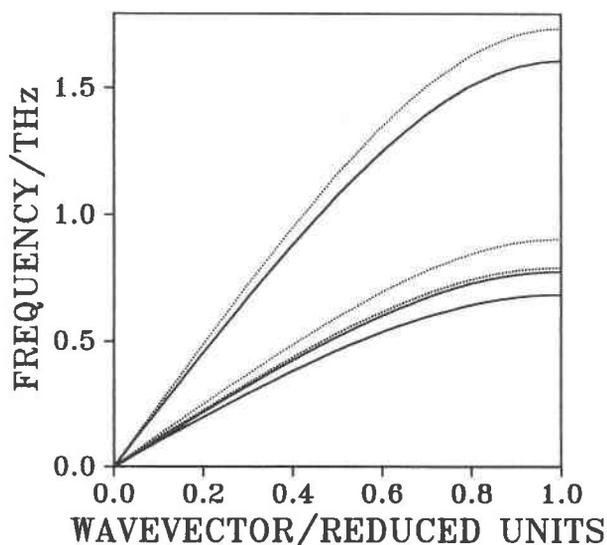
Fig. 2. Calculated longitudinal and transverse modes along (00ξ) of muscovite, at 0 K (dashed lines) and 300 K (solid lines).

TABLE 5. Experimental and calculated dielectric constants of muscovite

Static dielectric constant	Expt.* (orientationally averaged value)	0-K sim.	300-K sim.
ϵ_{11}	5.71	5.62	5.84
ϵ_{22}		5.30	5.50
ϵ_{33}		5.47	5.53
High-frequency dielectric constant	Expt.** (orientationally averaged value)	0-K sim.	300-K sim.
ϵ_{11}	2.43–2.54†	1.78	1.77
ϵ_{22}		1.83	1.82
ϵ_{33}		1.81	1.79

* Golop et al., 1968.
** Vaughan and Guggenheim, 1986.
† From refractive indices—muscovite measured at 488 nm.

imately sinusoidal, thereby suggesting that the associated atomic displacements are subject to restoring forces that act between nearest neighbor atoms only.

Dielectric properties. Although individual elements of the dielectric constant tensors have not been measured experimentally for muscovite or any other mica, bulk constants have been reported. These include a static dielectric constant (Golop et al., 1968) and a high-frequency dielectric constant derived from the values of the refractive index (Vaughan and Guggenheim, 1986). Our calculated values at both 0 and 300 K correspond to infinitely high and zero frequencies and are given in Table 5. The reasonable agreement of our calculated values with experiment supports the validity of our description of polarization in these materials.

Phlogopite

Structure. As with $2M_1$ muscovite, our modeling of $1M$ phlogopite shows general agreement with experimental data, although there are significant discrepancies. The simulated structures of phlogopite are in close agreement with experimental data (Hazen and Burnham, 1973; Knurr and Bailey, 1986), as shown in Table 6. As expected, the thermal expansion is anisotropic. The mean T-O distance is modeled well, although the O_{basal}-T-O_{apical} bond angles, τ, are predicted to be too small, again indicating a slightly over-repulsive K-O potential. The tetrahedral rotation angle, α, is underestimated, although it increases in the free-energy simulation.

As noted above, the departure from coplanarity of the basal O atoms, ΔZ, was correctly predicted to be significant for $2M_1$ muscovite. For $1M$ phlogopite, we correctly predict ΔZ to be neligible. The mean M1-O,OH and M2-O,OH bond lengths are slightly over estimated (by ~0.05 Å), although the octahedral flattening angles ψ(M1) and

TABLE 6. Comparison of simulated and experimental structural parameters of *1M* phlogopite

	Expt.*	Expt.**	0-K sim.	300-K sim.
Cell dimension				
a	5.308	5.316	5.387	5.395
b	9.190	9.221	9.324	9.334
c	10.155	10.282	10.054	10.134
β	100.08	99.9	97.03	96.47
Thickness				
Tet sheet	2.261	2.266	2.216	2.219
Oct sheet	2.125	2.143	2.192	2.193
Interlayer separation	3.352	3.454	3.354	3.439
Tet sheet				
Mean T-O	1.649	1.663	1.6208	1.622
τ	110.5	110.3	107.7	107.7
α	7.5	9.9	4.8	5.2
ΔZ	0.0	0.01	0.02	0.02
Oct sheet				
Mean M1-O-OH	2.063	2.073	2.137	2.140
M2-O, OH	2.064	2.072	2.135	2.137
ψ(M1)	59.0	58.9	59.2	59.2
ψ(M2)	59.0	58.9	59.1	59.1
O-H	—	0.76	0.97	0.97
Interlayer separation				
K-O$_{outer}$	3.3115	3.401	3.355	3.508
K-O$_{inner}$	2.969	2.950	2.998	3.022
Δ	0.343	0.451	0.357	0.485
Atomic coordinates (0-K sim.) in $C2/m$				
	x	y	z	
T1	0.0634	0.3338	0.2274	
M1	0.0000	0.5000	0.5000	
M2	0.0000	0.1745	0.5000	
K	0.0000	0.0000	0.0000	
O1 core	0.3064	0.2661	0.1682	
shell	0.3076	0.2635	0.1780	
O2 core	0.0061	0.5000	0.1666	
shell	0.0150	0.5000	0.1765	
O3 core	0.1277	0.3352	0.3940	
shell	0.1239	0.3348	0.3850	
OH	0.1158	0.0000	0.3818	
H	0.0690	0.0000	0.2844	

Note: All lengths in ångströms, angles in degrees. Simulations: $KMg_3AlSi_3O_{10}(OH)_2$.
* Hazen and Burnham (1973) $K_{0.85},Na_{0.15}(Mg_{3.0})Si_{2.95}Al_{1.05}O_{10}[(OH)_{0.7}F_{1.3}]$.
** Knurr and Bailey (1986) $K_{0.85},Na_{0.1}(Mg_{2.5},Fe^{3+}_{0.17},Mn^{2+}_{0.13},Al^{3+}_{0.11})Si_{2.8}Al_{1.2}$-$O_{10}[(OH)_{1.9}F_{0.1}]$.
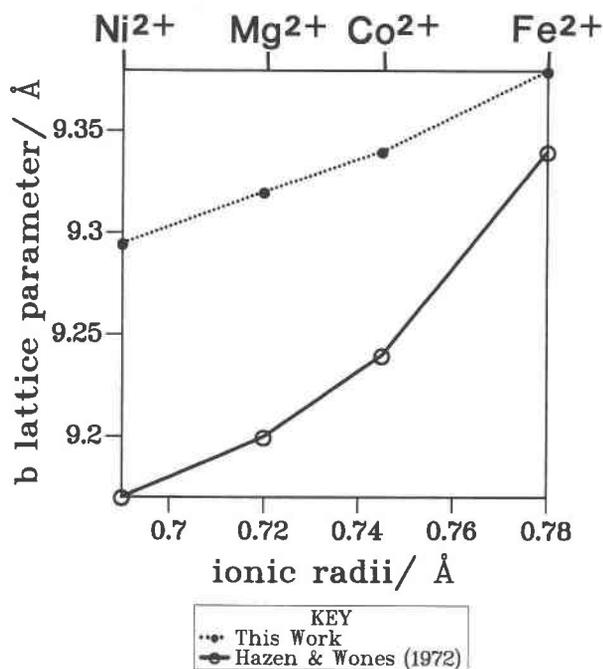
Fig. 3. Lattice parameter b vs. ionic radii for octahedrally substituted phlogopite.

ψ(M2) are in good agreement with experiment. The calculated O-H bond length has a more realistic value than that reported by Knurr and Bailey (1986). The discrepancies in the values of K-O$_{inner}$ and K-O$_{outer}$, and their difference, Δ, can be attributed to the inaccuracy in the modeling of the tetrahedral rotation angle, α. However, it is encouraging to note that the K-O bond lengths are significantly lengthened with the inclusion of temperature in the free-energy simulation, whereas the T-O, M1,M2-O, and O-H bond lengths are not.

Structure of octahedrally substituted phlogopite. A number of divalent cations (Ni, Mg, Cu, Co, Fe, Zn, Mn, Cd) can substitute into the octahedral sheet of the phlogopite structure. Energy minimization calculations were performed to investigate the effect of divalent octahedral cation substitutions on the structures of phlogopite analogues $(KR^{2+}_3AlSi_3)_{10}(OH)_2$. We continue to use hybrid species to represent tetrahedal cations, as the composition and Al-Si distribution of the tetrahedral sheet remains unchanged, with only the octahedral cation varying.

To allow reliable comparisons to be made among different octahedrally substituted phlogopite analogues, we required R^{2+}-O short-range potentials that were derived consistently, as discussed previously, where we noted our use of an earlier compilation of potentials (Lewis, 1984; Lewis and Catlow, 1985) (see Table 1). We recall that this set includes an alternative Mg-O potential to that used in all other simulations of phlogopite. However, a Cu^{2+}-O potential that is satisfactorily consistent with the other members of the set was not available, and the simulation of copper phlogopite has therefore not been performed.

In a study of cation substitution in phlogopite (Hazen and Wones, 1972), the effect of octahedral cation radii on unit-cell dimensions was examined. In addition, Hazen and Wones estimated values of tetrahedral rotation and octahedral flattening angles for various compositions. They found that it was possible for cations with ionic radii up to 0.76 Å to substitute with concentrations up to 100% into the octahedral sheet. Above this critical cation size the lateral dimensions of the octahedral sheet become larger than those of the tetrahedral sheet, resulting in instability, because distortions of the two sheets cannot overcome the sheet misfit. Cations with an ionic radius greater than 0.76 Å were found to fill the octahedral cation sites partially, with smaller cations occupying the remaining sites, ensuring that the overall average radius was below that of the critical value. Indeed, the existence of annite with Fe^{2+} (0.78 Å) in octahedral sites is attributed to the presence of small amounts of Fe^{3+} (0.63 Å) in the octahedral sites. Although Zn (0.75 Å) could enter into the octahedral sheet, the absence of natural and synthetic zinc phlogopite can be rationalized by the strong preference of Zn for tetrahedral coordination.

The calculated lattice energies predict the stability of phlogopite to be in the order Ni, Mg, Co, and Fe of octahedral cations and to be the same as that determined experimentally from thermal expansion and compression data (Hazen and Wones, 1978).

To test the ability of our simulation to model the behavior of different divalent octahedral cations on the unit-cell dimensions, we have made a detailed comparison of the results of our simulations with experimental data. Previous work has shown that the b axis of micas is sensitive to the size of the octahedral cation (Hazen and Wones, 1972; and Radoslovich and Norrish, 1962). The b axes of phlogopite with octahedral Ni, Mg, Co, and Fe for our simulated structures are in good agreement (within 2%) with those of experimental structures (Hazen and Wones, 1972) as shown in Figure 3. There is a slight overestimation of the magnitude of this axis, but we predict a linear increase with cation radius, in line with experimental results. A plot of the unit-cell volume as a function of the octahedral cation radius again shows excellent agreement between calculated structures and experimental data (see Fig. 4).

We now consider the relationship between the octahedral cation size and the tetrahedral rotation and octahedral flattening angles. The crystal structure of magnesium phlogopite is known accurately; hence values of α and ψ can be determined exactly using Equations 1 and 2 below:

$$\alpha = \tfrac{1}{2} \sum_i |120° - \text{mean O}_b\text{-O}_b\text{-O}_b \text{ angles}_i| \qquad (1)$$

$$\psi = \cos^{-1}(t_o/2d_o) \qquad (2)$$

where O$_b$-O$_b$-O$_b$ are individual angles between basal O atoms, t_o is the octahedral sheet thickness, and d_o is the average octahedral bond length. The detailed structures of the other octahedrally substituted phlogopite ana-
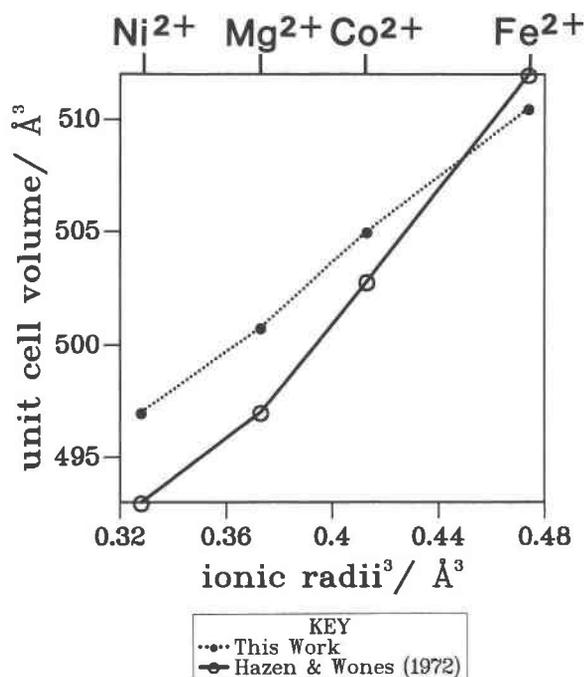
Fig. 4. Unit-cell volume vs. ionic radii cubed for octahedrally substituted phlogopite.

Fig. 5. Tetrahedral rotation angle (α) vs. ionic radii for octahedrally substituted phlogopite; a = Hazen and Burnham (1973), b = Joswig (1972), and c = Knurr and Bailey (1986).

logues are not known, therefore α and ψ must be estimated. From a knowledge of b and the average bond lengths, estimates of α and ψ have been made (Hazen and Wones, 1972) using Equations 3 and 4:

$$\alpha = \cos^{-1}(b/4 \cdot 2^{1/2} d_t) \qquad (3)$$

$$\psi = \sin^{-1}(b/3 \cdot 3^{1/2} d_o) \qquad (4)$$

where d_t and d_o are the average tetrahedral and octahedral bond lengths, respectively.

Experimental and simulated values of α and ψ as a function of octahedral cation radius are shown in Figures 5 and 6, respectively. The plots include the estimated values of Hazen and Wones (1972), three precise experimental values for magnesium phlogopite (Hazen and Burnham, 1973; Joswig, 1972; Knurr and Bailey, 1986), and values from our simulated structures.

The estimate of α by Hazen and Wones (1972) for magnesium phlogopite is in good agreement with the values determined precisely from detailed structural data, suggesting that Equation 3 can be used to predict accurately the values of α for other octahedrally substituted phlogopite. Our calculations reproduce the trend of decreasing α with increasing octahedral cation radius, although we underestimate this effect (see Fig. 5). The values of α given by Hazen and Wones range from ~9° for nickel phlogopite to 0° for iron phlogopite, whereas we predict ~7° for the former and ~5° for the latter.

The estimate of ψ by Hazen and Wones for magnesium phlogopite is, however, considerably smaller than the values determined precisely from detailed structural data, indicating that Equation 4 is inaccurate in predicting ψ
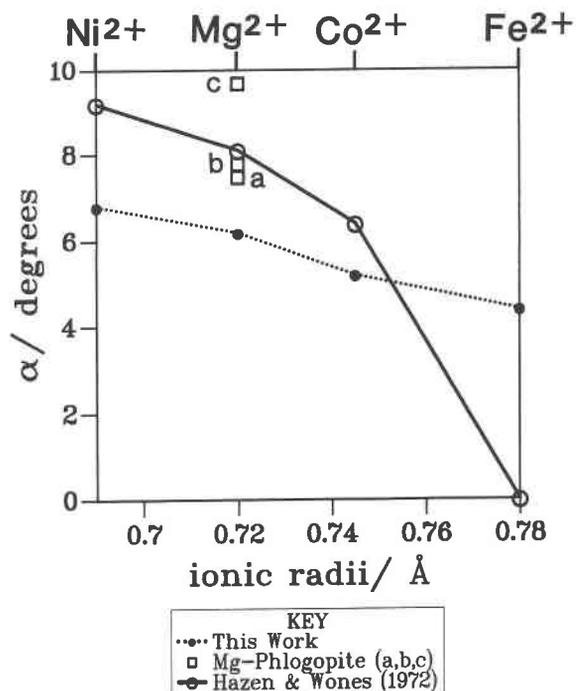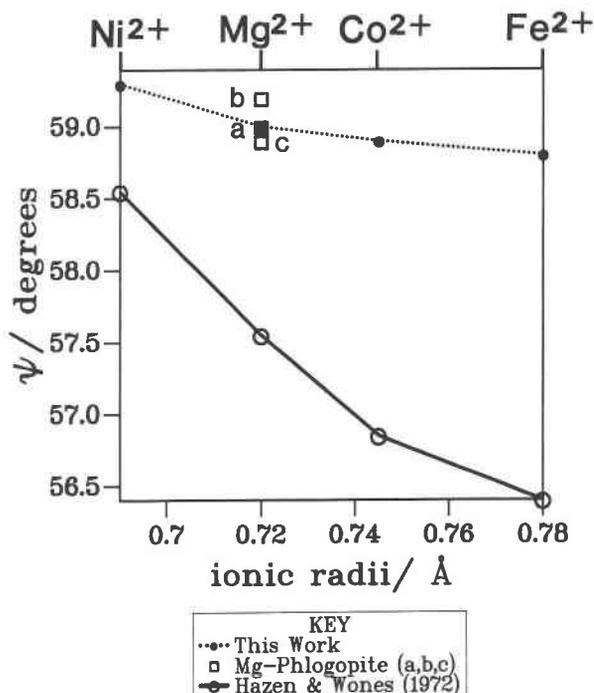
Fig. 6. Octahedral flattening angle (ψ) ionic radii for octahedrally substituted phlogopite; a = Hazen and Burnham (1973), b = Joswig (1972), and c = Knurr and Bailey (1986).

values for other octahedrally substituted phlogopite. The value of ψ for magnesium phlogopite, determined from our relaxed simulated structure, is in excellent agreement with the precise experimental values. Moreover, we predict the expected trend of decreasing ψ with increasing octahedral cation radius varying from $\sim 59.3°$ for nickel phlogopite to $\sim 58.5°$ for iron phlogopite (see Fig. 6). Thus, to summarize, we model the correct order of stability for octahedrally substituted phlogopite and, at least qualitatively, the effects of the octahedral cations on various structural parameters.

CONCLUSIONS

The results presented in this paper demonstrate clearly that energy minimization and free-energy minimization techniques can be used to investigate the properties of micas. We have shown the applicability of Born model potentials (which include three-body O-Si-O bond-bending terms) to this class of silicate. Moreover, all the short-range parameters used in this work were derived from studies of other materials, thus demonstrating that in this context the potentials used are transferable. Our calculations do, however, suggest that refinements of the potential models are needed to give accurate simulation of all structural details of micas.

Our study has also demonstrated the value of free-energy minimization techniques, which can model the thermal expansion of these materials and improve agreement between calculated and observed properties. Future challenges will include the modeling of hydration and phase stabilities within layer structured silicates.

REFERENCES CITED

Abbott, R.N., and Burnham, C.W. (1988) Polytypism in micas: A polyhedral approach to energy calculations. American Mineralogist, 73, 105–118.
Alexandrov, K.S., and Ryzhova, T.V. (1961) Elastic properties of rock-forming minerals, II, Layered silicates. Izvestia Akademie Nauk SSSR, Physics—Solid Earth, 1165–1168.
Bailey, S.W. (1975) Cation ordering and pseudosymmetry in layer silicates. American Mineralogist, 60, 175–187.
——— (1984) Review of cation ordering in micas. Clays and Clay Minerals, 32 (2), 81–92.
Born, M., and Huang, K. (1954) Dynamical theory of crystal lattices. Clarendon Press, Oxford, U.K.
Catlow, C.R.A. (1977) Point defect and electronic properties of uranium dioxide. Proceedings of the Royal Society of London, A353, 533–561.
Catlow, C.R.A., and Cormack, A.N. (1987) Computer modelling of silicates. International Review in Physical Chemistry, 6, 227–250.
Catlow, C.R.A., and Mackrodt, W.C. (1982) Theory of simulation methods for lattice and defect energy calculations in crystals. In C.R.A. Catlow and W.C. Mackrodt, Eds., Computer simulation of solids, p. 3–20. Springer-Verlag, Berlin.
Catlow, C.R.A., and Norgett, M.J. (1976) Lattice structure and stability of ionic materials. United Kingdom Atomic Energy Authority Report AERE-M2963.
Catlow, C.R.A., James, R., Mackrodt, W.C., and Stewart, R.F. (1982a)

Defect energies in α-aluminium oxide and rutile titanium dioxide. Physical Review B: Condensed Matter, 25, 1006–1026.
Catlow, C.R.A., Thomas, J.M., Parker, S.C., and Jefferson, D.A. (1982b) Simulating silicate structures and the structural chemistry of pyroxenoids. Nature, 295, 658–662.
Cebula, D.J., Owen, M.C., Skinner, C., Stirling, W.G., and Thomas, R.K. (1982) Observation of longitudinal acoustic phonons in layer-silicates by neutron inelastic scattering. Clay Minerals, 17, 195–200.
Cochran, W. (1973) The dynamics of atoms in crystal. Edward Arnold, London.
Collins, D.R., and Catlow, C.R.A. (1990) Interatomic potentials for micas. Molecular Simulation, 4, 341–346.
Dick, B.G., and Overhauser, A.W. (1958) Theory of the dielectric constants of alkali halide crystals. Physical Review, 112, 90–103.
Dove, M.T. (1989) On the computer modeling of diopside: Toward a transferable potential for silicate minerals. American Mineralogist, 74, 774–779.
Ewald, P.P. (1921) The calculation of optical and electrostatic lattice potentials. Annals of Physics (Leipzig), 64, 253–287.
Giese, R.F. (1974) Surface energy calculations for muscovite. Nature, 248, 580–581.
——— (1979) Hydroxyl orientations in 2:1 phyllosilicates. Clays and Clay Minerals, 27 (3), 213–223.
Golop, M.F., Nalivken, A.B., and Vokhemenstsev, A. (1968) A determination of dielectric constants of minerals. Shrencat Natures, 22, 3–18.
Gordon, R.G., and Kim, Y.S. (1972) A theory for the forces between closed-shell atoms and molecules. Journal of Chemical Physics, 56, 3122–3133.
Guggenheim, S., Chang, Y., and Koster van Groos, A.F. (1987) Muscovite dehydroxylation: High temperature studies. American Mineralogist, 72, 537–550.
Hazen, R.M., and Burnham, C.W. (1973) The crystal structure of one-layer phlogopite and annite. American Mineralogist, 58, 889–900.
Hazen, R.N., and Wones, D.R. (1972) The effect of cation substitution on the physical properties of trioctahedral micas. American Mineralogist, 57, 103–129.
——— (1978) Predicted and observed compositional limits of trioctahedral micas. American Mineralogist, 63, 885–892.
Hope, A.T.J. (1985) Experimental and theoretical studies on Pentasil zeolites. Ph.D. thesis, University College of London, London, England.
Jackson, R.A., and Catlow, C.R.A. (1988) Computer simulation studies of zeolite structure. Molecular Simulation, 1, 207–224.
Jenkins, M.D. (1982) Aspects of the chemistry of phyllosilicates and intercalation in vermiculites. In C.R.A. Catlow and W.C. Mackrodt, Eds., Lecture notes in physics, no. 116, p. 243–264. Springer-Verlag, Berlin.
Joswig, W. (1972) Neutronenbeugungsmessungen an einem 1M-Phlogopit. Neues Jahrbuch für Mineralogie Monatshefte, 1–11.
Knurr, R.A., and Bailey, S.W. (1986) Refinement of Mn-substituted muscovite and phlogopite. Clays and Clay Minerals, 34, 7–16.
Lasaga, A.C., and Gibbs, G.V. (1987) Applications of quantum mechanical potential surfaces to mineral physics calculations. Physics and Chemistry of Minerals, 14, 107–117.
Lewis, G. V. (1984) Computer modelling of mixed oxides. Ph.D. thesis, University College of London, London, England.
Lewis, G.V., and Catlow, C.R.A. (1985) Potential models for ionic oxides. Journal of Physics C, 18, 1149–1161.
Mackrodt, W.C., and Stewart, R.F. (1979) Defect properties of ionic solids. II. Point defect energies based on modified electron gas potentials. Journal of Physics C, 12, 431–449.
McCauley, J.W., and Newnham, R.E. (1971) Origin and prediction of ditrigonal distortions in micas. American Mineralogist, 56, 1626–1638.
Norgett, M.J., and Fletcher R.J. (1970) Fast matrix method for calculating the relaxation about defects. Journal of Physics C, L190–L192.
Parker, S.C. (1982) Computer modelling of minerals. Ph.D. thesis, University College of London, London, England.
Parker, S.C., and Price, G.D. (1985) A study of the structures and energetics of magnesium silicates. Physica, B131, 290–299.
——— (1989) Computer modelling of phase transitions in minerals. Advances in Solid State Chemistry, 1, 295–327.
——— (1990) Computer modeling of the structure and thermodynamic

properties of silicate minerals. In C.R.A. Catlow, S.C. Parker, and M.P. Allen, Eds., Computer modelling of fluids, polymers and solids, vol. 293, p. 405–492, N.A.T.O., Amsterdam.

Post, J.E., and Burnham, C.W. (1986) Ionic modeling of mineral structures and energies in the electron gas approximation: TiO_2 polymorphs, quartz, forsterite, diopside. American Mineralogist, 71, 142–150.

Price, G.D., Parker, S.C., and Leslie, M. (1987) The lattice dynamics of forsterite. Mineralogical Magazine, 51, 157–170.

Purton, J., and Catlow, C.R.A. (1990) Computer simulation of feldspar structures. American Mineralogist, 75, 1268–1273.

Radoslovich, E.W., and Norrish, K. (1962) The cell dimensions and symmetry of layer-lattice silicates I. Some structural considerations. American Mineralogist, 47, 599–616.

Rothbauer, R. (1971) Untersuchung eines $2M_1$-Muskovites mit Neutronenstrahlen. Neues Jahrbuch für Mineralogie Monatshefte, 143–154.

Sanders, M.J. (1984) Computer simulation of framework structured minerals. Ph.D. thesis, University College of London, London, England.

Sanders, M.J., Leslie, M., and Catlow, C.R.A. (1984) Interatomic potentials for SiO_2. Journal of the Chemical Society, Chemical Communication, 1271–1273.

Sangster, M.J.L., and Stoneham, A.M. (1981) Calculations of off-centre displacements of divalent substitutional ions in calcium oxide, strontium oxide and barium oxide from model potentials. Philosophical Magazine B, 43 (4), 597–608.

Saul, P., Catlow, C.R.A., and Kendrick, J. (1985) Theoretical studies of protons in sodium hydroxide. Philosophical Magazine B, 51, 107–117.

Takeda, H., and Morosin, B. (1975) Comparison of observed and predicted structural parameters of mica at high temperature. Acta Crystallographica, B31, 2444–2452.

Tosi, M.P. (1964) Cohesion of ionic solids in the Born model. In F. Seitz and K. Turnbull, Eds., Solid State Physics, vol. 16, p. 1–120. Academic Press, New York.

van Beest, B.W.H., Kramen, G.J., and van Santen, K.A. (1990) Force fields for silicates and aluminophosphates based on ab initio calculations. Physical Review Letters, 64 (16), 1955–1958.

Vaughan, M.T., and Guggenheim, S. (1986) Elasticity of muscovite and its relationship to crystal structures. Journal of Geophysical Research, 91 (B5), 4657–4664.

Wall, A., and Price, G.D. (1988) Computer simulation of the structure, lattice dynamics and thermodynamics of ilmenite-type $MgSiO_3$. American Mineralogist, 73, 224–231.

Ziman, J.M. (1964) Principles of the theory of solids (2nd edition). Cambridge University Press, Cambridge, U.K.

APPENDIX 1: CALCULATION OF ELASTIC CONSTANT TENSOR

Elastic constants C_{ij} are defined as the second derivatives (normalized to the unit-cell volume V_c) of the lattice energy with respect to the six independent strain components ($\epsilon_1 \ldots \epsilon_6$) used in the Voigt notation, i.e., $C_{ij} = (1/V_c)(\partial^2 U/\partial\epsilon_i\partial\epsilon_j)$. They are determined by first expanding the lattice energy (U) to the second order and assuming the equilibrium condition.

$$U(\mathbf{r}') = U(\mathbf{r}) + \tfrac{1}{2}\delta\mathbf{r}^T \cdot \mathbf{W}_{rr} \cdot \delta\mathbf{r} + \delta\mathbf{r}^T \cdot \mathbf{W}_{r\epsilon} \cdot \delta\epsilon + \tfrac{1}{2}\delta\epsilon^T \cdot \mathbf{W}_{\epsilon\epsilon} \cdot \delta\epsilon \quad (A1)$$

where $\delta\mathbf{r}$ and $\delta\epsilon$ are vectors of change in atomic positions and strains respectively. $\mathbf{W}_{rr}$, $\mathbf{W}_{r\epsilon}$, and $\mathbf{W}_{\epsilon\epsilon}$ are matrices whose elements are, respectively, the second derivatives of the lattice energy with respect to atomic coordinates, atomic coordinates and strain, and strains alone, i.e.,

$$W_{rr}^{ij} = \frac{\partial^2 U}{\partial r_i \partial r_j}; \quad W_{r\epsilon}^{ij} = \frac{\partial^2 U}{\partial r_i \partial \epsilon_j}; \quad W_{\epsilon\epsilon}^{ij} = \frac{\partial^2 U}{\partial \epsilon_i \partial \epsilon_j}. \quad (A2)$$

The derivatives may be calculated analytically if analytic forms of the interatomic potentials are employed.

Applying the equilibrium condition

$$\frac{\partial U}{\partial \mathbf{r}} = 0 \quad (A3)$$

to Equation A1 gives

$$\delta\mathbf{r} = -\mathbf{W}_{rr}^{-1} \cdot \mathbf{W}_{r\epsilon} \cdot \delta\epsilon. \quad (A4)$$

Substituting Equation A4 for $\delta\mathbf{r}$ for Equation A1 gives

$$U(\mathbf{r}') = U(\mathbf{r}) + \tfrac{1}{2}\delta\epsilon^T \cdot (\mathbf{W}_{\epsilon\epsilon} - \mathbf{W}_{\epsilon r} \cdot \mathbf{W}_{rr}^{-1} \cdot \mathbf{W}_{r\epsilon}) \cdot \delta\epsilon. \quad (A5)$$

The elastic constant matrix is then defined as

$$\mathbf{C} = (\mathbf{W}_{\epsilon\epsilon} - \mathbf{W}_{\epsilon r} \cdot \mathbf{W}_{rr}^{-1} \cdot \mathbf{W}_{r\epsilon})/V_c. \quad (A6)$$